Observation of mass-asymmetric fission of mercury nuclei in heavy ion fusion

E. Prasad,[*] D. J. Hinde,[†] K. Ramachandran,[‡] E. Williams, M. Dasgupta, I. P. Carter, K. J. Cook, D. Y. Jeung, D. H. Luong, S. McNeil, C. S. Palshetkar, D. C. Rafferty, C. Simenel, and A. Wakhle[§]
Department of Nuclear Physics, Research School of Physical Sciences and Engineering, The Australian National University, Canberra, ACT 2601, Australia

J. Khuyagbaatar
GSI Helmholtzzentrum für Schwerionenforschung, 64291 Darmstadt, Germany and Helmholtz Institute Mainz, 55099 Mainz, Germany

Ch. E. Düllmann
GSI Helmholtzzentrum für Schwerionenforschung, 64291 Darmstadt, Germany; Helmholtz Institute Mainz, 55099 Mainz, Germany; and Institute for Nuclear Chemistry, Johannes Gutenberg University Mainz, 55128 Mainz, Germany

B. Lommel and B. Kindler
GSI Helmholtzzentrum für Schwerionenforschung, 64291 Darmstadt, Germany
(Received 16 April 2015; published 8 June 2015)

Background: Mass-asymmetric fission has been observed in low energy fission of ^{180}Hg. Calculations predicted the persistence of asymmetric fission in this region even at excitation energies of 30–40 MeV.
Purpose: To investigate fission mass distributions by populating different isotopes of Hg using heavy ion fusion reactions.
Methods: Fission fragment mass-angle distributions have been measured for two reactions, ^{40}Ca+^{142}Nd and ^{13}C+^{182}W, populating ^{182}Hg and ^{195}Hg, respectively, using the Heavy Ion Accelerator Facility and CUBE spectrometer at the Australian National University. Measurements were made at beam energies around the capture barrier for the two reactions and mass ratio distributions were obtained using the kinematic reconstruction method.
Results: Asymmetric fission has been observed following the population of ^{182}Hg at an excitation energy of 22.8 MeV above the saddle point. A symmetric peaked mass ratio distribution was observed for ^{195}Hg nuclei at a similar excitation energy above the saddle point.
Conclusions: Mass-asymmetric fission has been observed in neutron deficient Hg nuclei populated via heavy ion fusion for the first time. The results are consistent with observations from beta-delayed fission measurements and provide a proof-of-principle for expanding experimental studies of the influence of shell effects on the fission processes.

DOI: 10.1103/PhysRevC.91.064605 PACS number(s): 25.70.Jj, 25.70.Gh, 25.85.−w

I. INTRODUCTION

Nuclear fission, a complex dynamic phenomenon, has been the topic of extensive theoretical and experimental studies since its discovery in 1939 [1,2]. To date, one of the greatest challenges in the field has arisen from observations of mass-asymmetric fission, in which the average mass split is not symmetric, unlike the liquid drop model prediction [3,4], but instead yields a distribution that can only arise from the influence of microscopic degrees of freedom.

Mass-asymmetric fission was first observed in the spontaneous and low-energy fission of actinide nuclei ($Z = 89$ to 103) [5]. The findings could be explained by considering fragment shell properties [4,5]—in this case, the doubly magic shell configuration at $Z = 50$ and $N = 82$. However, recent observations of mass asymmetric fission in β-delayed fission of isotopes of Hg [6–8] have suggested that shell structures other than those of the fragments themselves may play a vital role in shaping fission outcomes. In particular, the low yield of symmetric fission of ^{180}Hg, populating the semimagic ^{90}Zr has led to the speculation that shell properties of the fission fragments themselves, though significant in the potential energy surface near scission, must not play a major role [9] in determining the mass-split.

β-delayed fission has allowed mass distribution measurements for the most exotic (neutron-deficient) isotopes to date, with observations ranging from Hg to U. Unfortunately, the availability of nuclei undergoing β-delayed fission is constrained by the stringent conditions on β-decay branching ratios and Q values. Only certain nuclei are available for

[*]Permanent address: Department of Physics, School of Mathematical and Physical Sciences, Central University of Kerala, Kasaragod 671314, India; prasad.edayillam@anu.edu.au
[†]david.hinde@anu.edu.au
[‡]Present address: Nuclear Physics Division, Bhabha Atomic Research Centre, Mumbai 400085, India.
[§]Present address: National Superconducting Cyclotron Laboratory, Michigan State University, Michigan 48824, USA.

study, and the maximum excitation energy populated in these measurements is limited by the β-decay Q value of the parent nucleus [9]. To fully understand how fission mass distributions evolve as a function of compound nucleus (CN) excitation energy, N, and Z, we need a different approach.

In this work, we present the first experimental evidence that mass asymmetric fission in Hg isotopes can be observed in fission following heavy ion fusion. Mass distributions from heavy ion fusion reactions leading to ^{182}Hg ($N/Z = 1.28$) and ^{195}Hg (N/Z=1.44) are presented below, and discussed in the context of previous β-delayed fission measurements in the Hg region.

II. EXPERIMENTAL DETAILS

To examine the systematic behavior of fission properties of Hg isotopes, fission following heavy ion fusion reactions forming ^{182}Hg and ^{195}Hg was measured at the Australian National University's Heavy Ion Accelerator Facility.

The experimental setups were slightly different for the two reactions used, namely ^{40}Ca+^{142}Nd $\rightarrow$ ^{182}Hg and ^{13}C+^{182}W $\rightarrow$ ^{195}Hg, due to beam energy and kinematic requirements. Both setups are described below.

A. ^{40}Ca+^{142}Nd

For the ^{40}Ca+^{142}Nd reaction, pulsed ^{40}Ca beams (with a pulse separation of 107 ns and FWHM of 0.7–1.5 ns) from the 14UD Pelletron accelerator and superconducting linear post-accelerator were used to bombard the isotopically enriched $^{142}NdF_3$ target (thickness 400 μg/cm^2 with a 18 μg/cm^2 carbon backing facing downstream). The measurements were performed at laboratory energies (after correcting for energy loss in the target) of 167.7, 194.9, 199.9, 210.0, and 221.1 MeV. The target normal was oriented at 60° to the beam axis, which minimized the energy loss of the fission fragments in the target and also avoided shadowing of the detectors.

Fission fragments were detected using the ANU CUBE spectrometer [10], which consists of two large area position-sensitive multiwire proportional counters (MWPCs), each with an active area of 279 $\times$ 357 mm^2. These detectors provided timing, position (X and Y), and energy loss signals for each fission fragment. The fast timing information was obtained from the cathode foil of each detector and was measured with respect to the beam pulse.

For the ^{40}Ca+^{142}Nd measurement, the MWPC detectors were mounted at 45° (front detector) and 90° (back detector) scattering angles with respect to the beam direction. The detectors were placed such that the normal to the central foil of both detectors was at 180 mm from the target center, and at an azimuthal angle of 180° and 0° for the back and front detectors, respectively.

B. ^{13}C+^{182}W

Pulsed ^{13}C beams from the 14UD pelletron of 60.0, 63.0, and 66.0 MeV energy were used to bombard a ^{182}W target (25 μg/cm^2 in thickness, on a 15 μg/cm^2 carbon backing). For this experiment, the CUBE spectrometer MWPCs were placed such that the backward detector was at 135° with respect to the beam direction and the front detector remained at 45°. The target normal was oriented at 45° to the beam axis.

For both experiments, two silicon monitor detectors were mounted at $\theta = 30°$ at azimuthal angles of 90° and 270°, to measure the elastically scattered energy spectra and flux.

III. DATA ANALYSIS

A. Mass ratios

Using the kinematic coincidence method described below, absolute masses of each fragment are not determined, rather the mass ratio of the two fragments is determined. The calibrated positions and the time of flight information from the CUBE MWPCs were used to obtain the fragment velocities and center-of-mass angles assuming two-body kinematics [10,11]. Energy loss corrections were made for the beam particles as well as for the fission fragments produced in the reaction, assuming that interactions occurred at the center of the target. The fragment mass ratio (M_R) was then obtained by

$$M_R = \frac{m_1}{m_1 + m_2} = \frac{v_2}{v_1 + v_2}, \quad (1)$$

where m_1 and m_2 are the fragment masses at scission and v_1 and v_2 are the velocities in the center-of-mass frame for the fragments detected in the back and front detectors, respectively [12].

B. Mass-angle distributions

Before final mass ratio distributions were produced for each of the studied reactions, mass-angle distributions (plots of M_R versus $\theta_{\text{c.m.}}$) were extracted to investigate the presence of processes other than fusion-fission.

Mass-angle distributions (MAD) generally consist of groups from quasielastic, quasifission [13–16] and fusion-fission. In fusion-fission, the projectile and target nuclei undergo complete amalgamation after the capture process, resulting in a completely equilibrated compact system. Thus, the CN does not retain any memory of its entrance channel and undergoes fission after a significant time delay, typically ranging from several 10^{-20} to 10^{-16} s. Hence no memory is expected of the initial reaction partner masses and contact angle.

On the other hand, in quasifission, the system reseparates before reaching a completely shape-equilibrated system, often before 10^{-20} s, without completing a full rotation. For fast quasifission, a correlation between the fragment mass and emission angle is expected. Because this correlation can sometimes lead to mass asymmetric structures in the M_R distribution, MAD plots were generated in order to investigate the possible presence of quasifission.

The mass-angle distributions of fission from the ^{40}Ca+^{142}Nd and ^{13}C+^{182}W reactions are shown in Figs. 1 and 2, respectively. The CN excitation energies and $\frac{E_{\text{c.m.}}}{V_B}$ values are given on the top of each plot, where V_B is the capture barrier from a model [17] optimised for heavy systems. To maximize statistics, no limitation was placed on the ϕ acceptance of the detector at 135°.

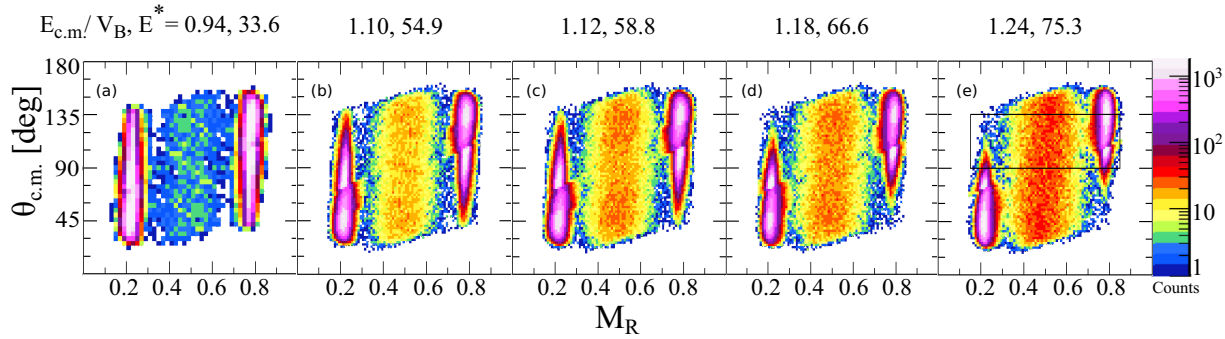

FIG. 1. (Color online) Experimental MAD scatter plots for ^{40}Ca+^{142}Nd reaction at different beam energies. The $\frac{E_{c.m.}}{V_B}$ values and CN excitation energies E^* are given at the top of each plot. The angular window used for producing the M_R distribution is indicated in (e).

For ^{40}Ca+^{142}Nd, the energy spectra of the elastic events recorded in the monitor detectors indicated that, unlike the ^{182}W target, the Nd target used in this measurement did not have a uniform thickness, possibly as a result of a beam-induced crack. The effect of this nonuniformity was also observed in the distributions of the deduced parallel component of the compound nucleus velocity ($V_{||}$) [10]. In order to minimize the effects on the mass angle and distributions originating from this nonuniformity, a narrow gate of width 0.8 mm/ns was imposed on the $V_{||}$ distribution, centered on the CN velocity (V_{CN}). Only the events within this gate were used for further analysis.

No significant correlation of fragment mass with angle was observed in the systems studied in this work when the tight gate was applied around $V_{||} = V_{CN}$ for the ^{40}Ca+^{142}Nd reaction. Without this gate, a spurious mass-angle correlation was visible, arising from the large energy (velocity) losses of the heavy backward angle fragments in the thicker parts of the target, which generated events apparently having very large M_R (>0.6) at large $\theta_{c.m.}$.

C. Generating M_R distributions

The final M_R distributions were obtained by projecting the experimental MADs shown in Figs. 1 and 2 onto the M_R axis. An angular window ($\Delta\theta$) of width 45° has been selected for both the reactions (90° < $\Delta\theta$ < 135° for ^{182}Hg and 120° < $\Delta\theta$ < 165° for ^{195}Hg) to avoid biasing of data due to the geometrical limits of the detectors' angular acceptance. These are shown as rectangles in Figs. 1(e) and 2(c). The angular windows selected (including no data forward of 90°) eliminate any mirrored data in the final M_R distributions. This rules out the possibility of a spurious asymmetric appearance of the M_R distribution, such as could originate while mirroring an M_R distribution where the M_R peak was not centered at $M_R = 0.5$.

IV. RESULTS

The M_R distributions of the fragments from the reactions leading to ^{182}Hg and ^{195}Hg are shown in Figs. 3(a) and 3(b). In the panels, the counts at different excitation energies were scaled as indicated in Fig. 3.

For the ^{13}C+^{182}W reaction the M_R distributions are peaked at mass symmetry for all energies studied. Within the experimental statistics, the distributions are consistent with a Gaussian form. Although a similar trend is observed at most beam energies for the ^{40}Ca+^{142}Nd reaction, a strong mass-asymmetric component is observed at the lowest CN excitation energy of $E^* = 33.6$ MeV. According to a recent calculation [18], the fission barrier height of ^{182}Hg is 10.85 MeV at zero angular momentum. Hence, the available excitation energy

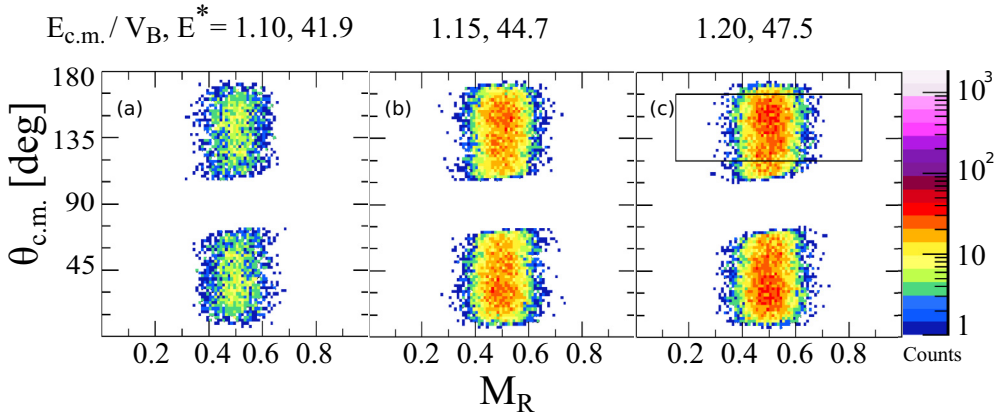

FIG. 2. (Color online) Experimental MAD scatter plots for ^{13}C+^{182}W reaction at different beam energies. The angular window used for producing the M_R distribution is indicated in (c).

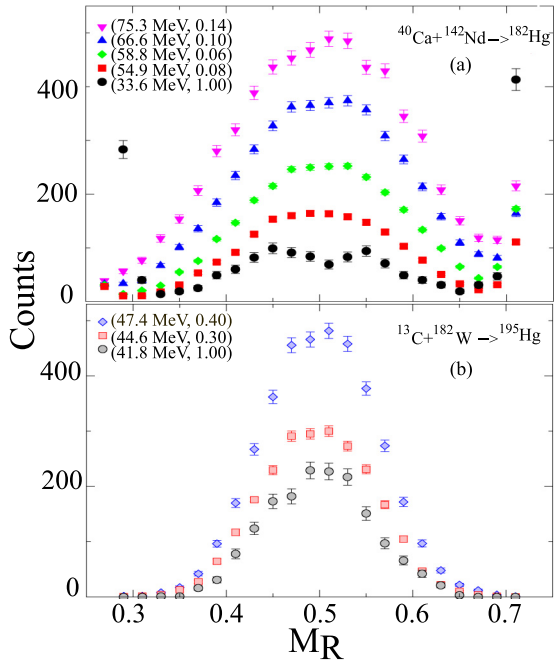

FIG. 3. (Color online) The M_R distributions of fission from (a) ^{40}Ca+^{142}Nd and (b) ^{13}C+^{182}W reactions at different CN excitation energies. The yields are scaled to show different energies in a single plot. The excitation energy and scaling factors used are shown in parentheses.

above the saddle point for this nucleus is 22.8 MeV at the lowest measured energy. The fission barrier height of 18.79 MeV [18] for ^{195}Hg indicates that this nucleus would be 23.0 MeV and 28.6 MeV above the saddle point when the CN excitation energies were 41.8 MeV and 47.4 MeV, respectively. The similarities in the excitation energies suggest that the observed asymmetric fission in ^{182}Hg and absence in ^{195}Hg should be due to the difference in the dynamical evolution of neutron deficient (^{182}Hg) and neutron rich (^{195}Hg) CN of the same element.

The widths of the fission fragment M_R distributions for all reactions and excitation energies measured in this work have been quantified by fitting the data with a Gaussian function. The standard deviations (σ_{MR}) are shown in Table I. The σ_{MR} values increase with increasing beam energy. The absence of a significant mass angle correlation for the measured MADs at all energies rules out fast quasifission as a major contributor in the ^{40}Ca+^{142}Nd measurements, as discussed in Sec. III B. However, some quasifission events with longer sticking times could contribute to the observed mass ratio distributions. In particular, quasifission could contribute to the increasing mass widths found at higher beam energies and corresponding high angular momenta. The smallest contribution would be expected at the lowest beam energy (lowest E^*).

TABLE I. Single Gaussian widths (σ_{MR}) obtained for the M_R distributions for different systems studied in this work. The CN excitation energy E^* and excitation energy above the saddle point E^*_{saddle} are also shown.

Reaction	CN	E^* (MeV)	E^*_{saddle} (MeV)	σ_{MR}
^{40}Ca+^{142}Nd	^{182}Hg	33.6	22.8	0.0862 ± 0.0030
		54.9	44.1	0.0824 ± 0.0007
		58.8	48.0	0.0877 ± 0.0006
		66.6	55.8	0.0950 ± 0.0008
		75.3	64.5	0.1006 ± 0.0010
^{13}C + ^{182} W	^{195}Hg	41.8	23.0	0.0626 ± 0.0013
		44.6	25.8	0.0617 ± 0.0004
		47.4	28.6	0.0609 ± 0.0004

V. DISCUSSION

This discussion will focus on the asymmetric mass-ratio distributions observed in the ^{40}Ca+^{142}Nd reaction at $E^* = 33.6$ MeV. We will investigate how this result compares to the previous observation in the Hg region from β-delayed fission, and its significance in terms of future exploration of mass-asymmetric fission using heavy ion fusion reactions.

A. A comparison of β-delayed fission of ^{180}Hg and fission following fusion of ^{40}Ca+^{142}Nd

In the mass-asymmetric fission of ^{180}Hg observed in β-delayed fission [6,8], the fissioning nuclei were populated at very low excitation energies. Figure 4 shows the result of the present measurement, of fission following formation of ^{182}Hg, in the fusion of ^{40}Ca with ^{142}Nd, at $E^* = 33.6$ MeV and that for ^{180}Hg populated at $E^* = 10.44$ MeV [6,8]. For this figure, the fragment mass distribution reported in Ref. [8] has been converted into a mass ratio distribution, shown in Fig. 4(a). The fission yields were reported with a bin size of 2 amu in Ref. [8]. We also show these data with a bin size of 4 amu for comparison with our data for the ^{40}Ca+^{142}Nd reaction [shown in Fig. 4(b)] which is binned into 50 channels over the full mass ratio range from 0 to 1, corresponding to a mass width of 3.64 amu.

Figures 4(a) and 4(b) show striking similarities in the asymmetric nature of the mass split spectra, and the M_R values of the peak positions. The asymmetric peaks in the fission of ^{180}Hg were reported to be centered around ^{80}Kr and ^{100}Ru, translating to M_R values 0.44 and 0.56 for the light and heavy fragments, respectively. The asymmetric peaks observed in the ^{40}Ca+^{142}Nd reaction are consistent with these M_R values.

The relatively low fissility of ^{182}Hg suggests that the observed fission could be dominated by first chance fission and the contribution from fission following evaporation of one or more particles (multichance fission) is negligible. However, estimated pre-scission neutron multiplicities based on systematics reported in the literature ($n_{pre} = 0.51$ using systematics from Ref. [19], and 0.82 using systematics from Ref. [20]) suggest that the contribution from multichance fission may be significant.

We have investigated the scenario that fission of ^{180}Hg contributes to the mass-asymmetric fission we have observed. To explore this possibility, the area under the two distributions shown in Figs. 4(a) and 4(b) were normalized, and a fraction of the experimental fission mass ratio distribution from ^{180}Hg

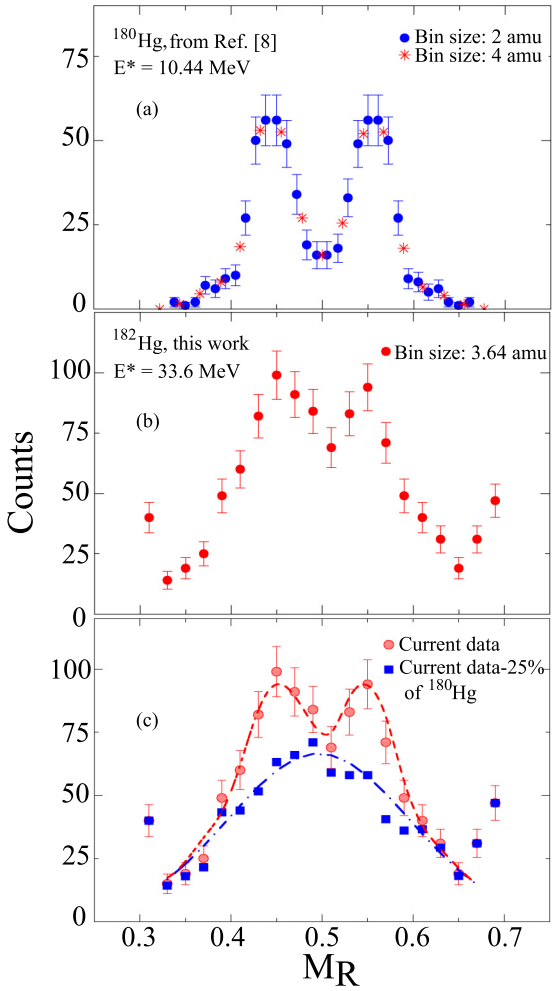

FIG. 4. (Color online) (a) The fragment M_R distributions of ^{180}Hg reported in Ref. [8] at $E^* = 10.44$ MeV. The mass distribution in Ref. [8] was reported with a bin size of 2 amu. The same distribution (scaled) is also shown with a bin size of 4 amu for comparison. (b) M_R distributions of the fission observed following the reaction ^{40}Ca+^{142}Nd at $E^* = 33.6$ MeV with a bin size of 3.64 amu. (c) M_R distribution obtained by subtracting 25% contribution from the fission of ^{180}Hg. A Gaussian fit to this distribution is shown using the dot-dashed line (blue). Dashed line (red) represents the sum of Gaussian fit values and 25% contribution from (a).

was subtracted from the experimental M_R distribution from the ^{40}Ca+^{142}Nd reaction to obtain a smooth symmetric-peaked distribution. Subtracting a 25% contribution from ^{180}Hg leads to the Gaussian shaped distribution shown by square points in Fig. 4(c). This could be well fitted by a Gaussian function centered at $M_R = 0.5$, as shown by the dot-dashed line. The sum of the Gaussian fit and the 25% fraction of ^{180}Hg asymmetric fission is shown by the dashed line. These results show that a contribution of a 25% from fission of ^{180}Hg, that would occur after evaporation of two neutrons from the CN, could explain the mass-asymmetric fission observed in this work.

However, at this stage we cannot exclude the possibility that the mass asymmetric fission could all originate from fission at higher excitation energies (e.g., first-chance fission of ^{182}Hg). Below, we will discuss theoretical predictions that are consistent with the observed mass asymmetric fission originating from the CN ^{182}Hg, or at least from the higher E^*, and explore how these predictions compare with our experimental results.

B. Theoretical considerations

The process of fission is affected by a subtle interplay of macroscopic and microscopic effects during the transition of the CN from the ground state deformation to the scission point. It has been widely accepted that the spherical doubly magic nucleus ^{132}Sn, with $Z = 50$ and $N = 82$, strongly influences the mass distributions in fission of actinide nuclei. In low energy asymmetric fission of ^{180}Hg, the low yield of symmetric fission with fragments close to the semimagic configuration $Z = 40$ and $N = 50$, corresponding to ^{90}Zr, indicates that shell structure in the fission fragments themselves is not very significant in deciding the mass distribution.

The origin of the mass-asymmetric mass split in low energy fission of light Hg isotopes was qualitatively explained [6,9,21] using recent potential energy surface calculations. According to these calculations, the light Hg isotopes possess a single mass-asymmetric saddle point leading from the ground-state minimum towards a shallow mass-asymmetric valley. A deep mass-symmetric valley beyond the saddle point is separated from the shallow asymmetric shallow by a ridge which disappears before the scission point. This symmetric valley is not directly accessible from the ground state due to the high barrier along a mass-symmetric path to scission. This potential energy surface suggests [6] that mass-asymmetric fission results when the system starts to follow the shallow mass-asymmetric valley in elongation. Whilst the ridge separating this valley from the deeper symmetric valley vanishes near scission, the mass degree of freedom can become frozen, since a well-developed neck with a small radius can prevent further mass flow before scission.

Recently, Möller *et al.,* [22] performed calculations of fission yields for neutron-deficient Hg isotopes (^{174}Hg-^{188}Hg) using a Brownian shape motion (BSM) treatment. Emphasizing the imperfections of phenomenological and static-only approaches in explaining the recent results in the Hg region, the authors emphasized the necessity to include in calculations the shape evolution over the potential energy surface from the ground state all the way to the separated fragments. These calculations predicted a flat mass distribution for the lightest (^{174}Hg) isotope considered, with a transition towards mass symmetry with decreasing excitation energy. Crucially, the calculations predicted the occurrence of mass-asymmetric fission in heavier Hg isotopes (from ^{176}Hg to ^{188}Hg), for CN excitation energies as high as 40 MeV. Our experimental results are compared with the BSM predictions for ^{182}Hg in Fig. 5. While both show mass-asymmetric fission, the mass centroids of the asymmetric peaks are different, as was also noted for low energy fission of ^{180}Hg [22]. A considerable mismatch of the full width at half-maximum of the asymmetric peaks was also observed, which was proposed to be due to the absence of confining fission valley walls in the Hg region [21].

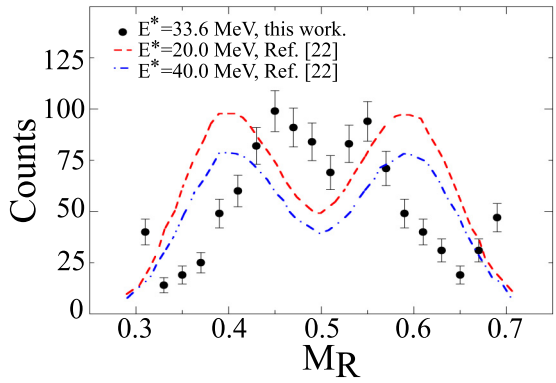

FIG. 5. (Color online) Experimental fission fragment M_R distribution for ^{40}Ca+^{142}Nd at $E^* = 33.6$ MeV is compared with Möller's predcitions for the same compound nucleus ^{182}Hg at $E^* = 20$ MeV (red dashed line) and 40 MeV (blue dot-dashed line). The mass distributions obtained using the Brownian shape motion treatment in Ref. [22] were converted to M_R distributions and scaled for this plot.

Calculations based on finite-temperature density functional theory have also predicted the occurrence of mass-asymmetric fission in the neutron deficient Hg region at higher CN excitation energy. It was reported in Ref. [23] that the barrier to symmetric fission gradually lowers with increasing excitation energy. However, this variation is predicted to be very gentle [23]. The calculations predict that asymmetric fission should dominate in the neutron deficient Hg region at excitation energies up to 30 MeV.

Turning to fission of more neutron-rich Hg isotopes, the fission fragment mass distribution for ^{198}Hg was measured [24] at about 10.9 MeV of excitation energy above the saddle point: a flat topped mass distribution was observed. Symmetric distributions centered at $M_R = 0.5$ were observed for ^{195}Hg in the present work. The authors in Ref. [21] observed that the shallow asymmetric valley extending from saddle to elongated shapes with small neck exists only for Hg isotopes with mass numbers between 180 and 190. The absence of this feature for ^{195,198}Hg could explain the absence of a strong mass-symmetric fission mode for these nuclei.

C. Outlook

In this work, we observed mass-asymmetric fission following formation of ^{182}Hg at 33.6 MeV excitation energy. Superficially, this would seem to support the persistence of shell effects up to this excitation energy. Various theoretical models (see Sec. V B) predict the presence of asymmetric fission up to excitation energies of 30–40 MeV. However, a 25% contribution from third chance fission (of ^{180}Hg) could also explain the observed results, since an empirical calculation (see Sec. V A) based on this assumption reproduces the observed M_R distribution. Hence, from the current results, we cannot make any definitive statement about the nature of shell effects at high excitation energies. While the mass ratio distributions for ^{40}Ca+^{142}Nd reactions at higher excitation energies measured in this work show a rather flat-topped shape (indicating that some asymmetric component may underlie the main symmetric peak), the signature of mass asymmetric fission is much weaker, unlike at the lowest energy.

The results reveal a promising opportunity to explore directly the new mode of fission in the light Hg region and beyond, using heavy ion fusion-fission. While beta-delayed fission offers a precise means of studying low-energy fission, it is limited by the availability of nuclei that undergo β-delayed fission, as well as the statistical limitations of the method. Heavy ion fusion reactions remove both limitations, in exchange for a somewhat more complicated interpretation of the fission processes contributing to observed structures in M_R distributions.

VI. SUMMARY AND CONCLUSIONS

In this work we have presented the fission fragment mass ratio distributions and mass-angle correlations for the ^{40}Ca+^{142}Nd and ^{13}C+^{182}W reactions, forming neutron-poor and relatively neutron-rich isotopes of Hg. The mass-angle correlations ruled out a significant influence of fast quasifission. For the ^{13}C+^{182}W reaction the fission M_R distributions were found to be peaked at mass symmetry (within experimental uncertainties) at all energies. The most interesting result was the observation of a strong component of mass-asymmetric fission for the ^{40}Ca+^{142}Nd reaction at $E^* = 33.6$ MeV (approximately 22.8 MeV above the zero-angular momentum saddle point energy). The mass-asymmetric structure observed has been compared to previous measurements of low energy (β-delayed) fission of ^{180}Hg. Both mass distributions have asymmetric peaks centered at similar values.

The existence of asymmetric fission at $E^* = 30$–40 MeV has recently been predicted by different theoretical approaches [22,23]. Our results provide the first experimental evidence of asymmetric fission originating from heavy ion fusion-fission in the light Hg region. We have shown that our measurement for ^{182}Hg can also be due to a 25% contribution from last-chance fission (of ^{180}Hg). More detailed measurements with finer energy steps and higher statistics will be valuable to understand the role of multichance fission in this mass region.

In the case of Hg, it would be interesting to explore the transition region from asymmetric to symmetric fission in more detail. In particular, questions remain about the threshold energy at which symmetric fission becomes dominant and understanding the dynamics over the potential energy surface which determines the evolution from the equilibrium deformation to scission.

More generally, the observation of mass-asymmetric fission following heavy ion fusion at reasonably high excitation energies offers a new avenue for exploring this *new mode* of fission. By choosing different projectile-target combinations, a wide range of nuclei may be populated in heavy ion collisions, opening up areas of the nuclear chart otherwise inaccessible to fission mass distribution measurements. Combined with large area fission detectors such as in the ANU CUBE spectrometer, better statistics may be achieved more quickly in comparison to β-delayed fission studies, which demand longer periods of data acquisition to achieve similar statistics.

Thus heavy ion fusion-fission offers an experimental approach complementary to beta-delayed fission following heavy ion fusion. Through a comprehensive exploration of this region of mass asymmetric fission, accessed via a combination of experimental techniques, we may be able to refine the existing models of fission such that a single model could consistently explain the fission of all nuclei across the nuclear chart.

ACKNOWLEDGMENTS

The authors are grateful to the accelerator staff of the ANU Heavy Ion Accelerator Facility for their excellent support during the experiments. The authors acknowledge support from the Australian Research Council through grants no. FL110100098, FT120100760, DP130101569, DP140101337, and DE140100784.

[1] O. Hahn and F. Strassman, Naturwiss **27**, 11 (1939).
[2] L. Meitner and O. R. Frisch, Nature **143**, 239 (1939).
[3] N. Bohr and J. A. Wheeler, Phys. Rev. **56**, 426 (1939).
[4] L. Meitner, Nature **165**, 561 (1950).
[5] R. Vandenbosch and J. R. Huizenga, *Nuclear Fission* (Academic, New York, 1973).
[6] A. N. Andreyev, J. Elseviers, M. Huyse, P. Van Duppen, S. Antalic, A. Barzakh, N. Bree, T. E. Cocolios, V. F. Comas, J. Diriken *et al.*, Phys. Rev. Lett. **105**, 252502 (2010).
[7] V. Liberati, A. N. Andreyev, S. Antalic, A. Barzakh, T. E. Cocolios, J. Elseviers, D. Fedorov, V. N. Fedoseeev, M. Huyse, D. T. Joss *et al.*, Phys. Rev. C **88**, 044322 (2013).
[8] J. Elseviers, A. N. Andreyev, M. Huyse, P. Van Duppen, S. Antalic, A. Barzakh, N. Bree, T. E. Cocolios, V. F. Comas, J. Diriken *et al.*, Phys. Rev. C **88**, 044321 (2013).
[9] A. N. Andreyev, M. Huyse, and P. Van Duppen, Rev. Mod. Phys. **85**, 1541 (2013).
[10] D. J. Hinde, M. Dasgupta, J. R. Leigh, J. C. Mein, C. R. Morton, J. O. Newton, and H. Timmers, Phys. Rev. C **53**, 1290 (1996).
[11] R. Rafiei, R. G. Thomas, D. J. Hinde, M. Dasgupta, C. R. Morton, L. R. Gasques, M. L. Brown, and M. D. Rodriguez, Phys. Rev. C **77**, 024606 (2008).
[12] R. du Rietz, E. Williams, D. J. Hinde, M. Dasgupta, M. Evers, C. J. Lin, D. H. Luong, C. Simenel, and A. Wakhle, Phys. Rev. C **88**, 054618 (2013).
[13] W. J. Świątecki, Phys. Scr. **24**, 113 (1981).
[14] J. P. Blocki, H. Feldmeier, and W. J. Świąteck, Nucl. Phys. A **459**, 145 (1986).
[15] D. J. Hinde, M. Dasgupta, and A. Mukherjee, Phys. Rev. Lett. **89**, 282701 (2002).
[16] P. Möller and A. J. Sierk, Nature **422**, 485 (2003).
[17] W. J. Świątecki, K. Siwek-Wilczyńska, and J. Wilczyński, Phys. Rev. C **71**, 014602 (2005).
[18] P. Möller, A. J. Sierk, T. Ichikawa, A. Iwamoto, R. Bengtsson, H. Uhrenholt, and S. Åberg, Phys. Rev. C **79**, 064304 (2009).
[19] H. Baba, A. Shinohara, T. Saito, N. Takahashi, and A. Yokoyama, J. Phys. Soc. Jpn. **66**, 998 (1997).
[20] M. G. Itkis and A. Ya. Rusanov, Phys. Part. Nucl. **29**, 160 (1998).
[21] T. Ichikawa, A. Iwamoto, P. Möller, and A. J. Sierk, Phys. Rev. C **86**, 024610 (2012).
[22] P. Möller, J. Randrup, and A. J. Sierk, Phys. Rev. C **85**, 024306 (2012).
[23] J. D. McDonnell, W. Nazarewicz, J. A. Sheikh, A. Staszczak, and M. Warda, Phys. Rev. C **90**, 021302(R) (2014).
[24] M. G. Itkis, V. N. Okolovich, and G. N. Smirenkin, Nucl. Phys. A **502**, 243c (1989).